JOURNAL OF MATERIALS SCIENCE 29 (1994) 1901–1909

Effect of the loading system on the stress distribution in the fully embedded fibre pull-out test

C. Y. YUE, H. C. LOOI
School of Mechanical and Production Engineering, Nanyang Technological University, Nanyang Avenue, Singapore 2263

The effect of the loading system on the stress distribution in the fully embedded fibre pull-out test has been considered. Tests on a fully embedded fibre specimen resemble more closely conditions within a composite system. Both the top-restrained and fixed-bottom test configurations were considered. Effects of relative moduli and radii of the matrix and the fibre on stress distribution were considered. The influence of these on the maximum debond force and on the location of debonding crack initiation within the specimen were also determined.

1. Introduction

It is well known that the mechanical properties of a composite depend on its interfacial properties. The interfacial properties are characterized by interfacial parameters such as the interfacial shear strength, τ_i, matrix shrinkage pressure on the fibre, P_o, coefficient of friction, μ, and the interfacial toughness, G_i. A number of experimental techniques has been developed to determine these interfacial parameters including the single-fibre pull-out, fibre fragmentation and fibre push-out (indentation) tests. The simple single-fibre pull-out test, which has the advantage that it can be directly applied to any fibre–matrix system of interest, is the subject of this work.

Theoretical pull-out models have been developed on either a strength-based [1–5] or a fracture-based approach [6–9]. Based on experiments from the glass fibre–polypropylene system, Yue and Cheung [10] showed that the applicability of fracture-based model to model pull-out systems was dependent on the specimen geometry. In contrast, the applicability of the strength-based model considered was independent [10] of the geometry of the model pull-out specimen. It has also been shown theoretically [4, 11] that the maximum debonding force in a pull-out test is affected by the loading method. However, the above work consider specimens in which the fibers extend along the length of the matrix such that the broken fibre ends are exposed.

A recent strength-based model [5] considers pull-out specimens in which the fibre is fully embedded within the matrix. The fixed-bottom loading condition (see Fig. 1) was considered. After the initial debonding crack initiation, progressive debonding was assumed to occur. The maximum debonding force was determined by the total force to overcome frictional pull-out and to cause further crack debonding. This model could be used [12] to determine the interfacial parameters for fibre composite systems. The model could also predict [5] the point of interfacial crack initiation and account [12] for the two-way debonding observed in some pull-out specimens. However, the restrained-top loading condition (see Fig. 1) has not been considered in the above model.

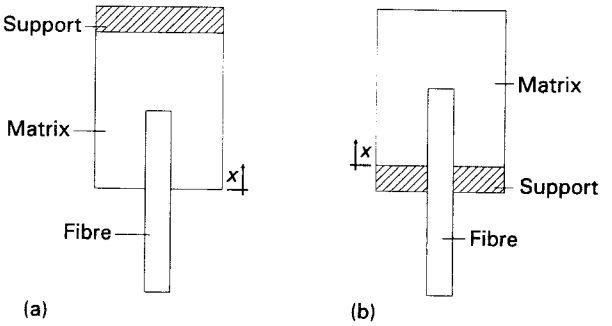

Figure 1 Type of specimen loading. (a) Fixed bottom, (b) restrained top.

The present work aimed to elucidate the effect of the loading method on the new [5] model. In particular, the influence of loading method, relative fibre/matrix moduli, and specimen geometry on the point of interfacial crack initiation, stress distribution and maximum pull-out load were examined.

2. Analysis

There are two possible loading conditions in a pull-out test. These are depicted in Fig. 1 and are (a) the fixed bottom (FBC), and (b) the restrained top (RTC) conditions. They have also been referred to as the fully supported and freely supported conditions, respectively. In the FBC, the load is applied by pulling the free end of the fibre whilst gripping the matrix in a region away from the fibre-embedded end. The complete derivation of the model under such a loading condition is given elsewhere [5].

0022–2461

The analysis for a similar model, which assumes a strength-based criterion for debonding crack initiation and takes into consideration the increasing contribution of the pull-out component to the debonding load as interfacial debonding progresses, will now be considered for the RTC condition for a fully embedded specimen.

2.1. Stresses at the interface

Consider the application of a load, F_p, to a specimen in the RTC. The specimen will deform elastically as shown in Fig. 2. The shear force on a fibre element dx is equal to $2\pi a\tau_x dx$. The stress across the fibre end is assumed to be negligible. By assuming the shear force to be linearly distributed in the y direction such that the shear force at the circumference of the matrix block is zero, it can be shown (see Appendix I) that the expressions for the interfacial shear stress distribution, τ_x, and the tensile stress on the matrix, σ_{mx}, and fibre, σ_{fx}, are

$$\tau_x = \frac{F_p}{2\pi a}\left[\frac{-\alpha(1+\psi)\cosh\alpha(L-x)+\alpha\psi\cosh\alpha x}{\sinh\alpha L}\right] \quad (1)$$

$$\sigma_{mx} = \frac{F_p}{\pi(b^2-a^2)}\left[\frac{(1+\psi)\sinh\alpha(L-x)+\psi\sinh\alpha x}{\sinh\alpha L}-\psi\right] \quad (2)$$

$$\sigma_{fx} = \frac{F_p}{\pi a^2}\left[1+\frac{(1+\psi)\sinh\alpha(L-x)+\psi\sinh\alpha x}{\sinh\alpha L}-\psi\right] \quad (3)$$

where

$$\alpha = \left\{2G_m\Big/\left\{(b^2-a^2)\left[\left(\frac{b}{b-a}\right)\ln\left(\frac{b}{a}\right)-1\right]\right\}\right\}\left[\frac{E_m(b^2-a^2)+E_f a^2}{E_f E_m a^2}\right]^{1/2}$$

$$\psi = \frac{E_m(b^2-a^2)}{E_m(b^2-a^2)+E_f a^2}$$

x is the distance from the emergent end, b and a are the radii of the matrix block and the fibre, respectively, G_m, E_m are the shear and elastic modulus of matrix, and E_f is the elastic modulus of the fibre.

2.2. Pull-out force for interfacial debonding

In general, interfacial debonding in a specimen under the RTC occurs at the fibre emergent end (i.e. at $x = 0$ in Fig. 1). Utilizing a strength-based criterion, debonding initiates when the interfacial shear stress, τ_x, in Equation 1 reaches the interfacial bond strength, τ_i. Therefore, from Equation 1, the pull-out force, F_i, required to initiate debonding at $x = 0$ is

$$F_i = \frac{2\pi a\tau_i\sinh\alpha L}{-\alpha(1+\psi)\cosh\alpha L+\alpha\psi} \quad (4)$$

Once the debonding crack has initiated, the stresses at the interface will be redistributed such that the stress at the crack tip falls below τ_i. Further crack propagation will only occur if the stress at the crack tip reaches τ_i through an increase of the applied load.

The pull-out force, F_p, required to ensure further progressive interfacial crack debonding comprises two components, namely, the force F_{uy} required to debond the remaining bonded length, l_u, of fibre, and the force, F_f, required to overcome frictional pull-out due to matrix shrinkage onto the debonded length, l_d, of the fibre. The force F_{uy} required to propagate the crack front is obtained by substituting L in Equation 4 with l_u so that

$$F_{uy} = \frac{2\pi a\tau_i\sinh\alpha l_u}{-\alpha(1+\psi)\cosh\alpha l_u+\alpha\psi} \quad (5)$$

For a rigid system, in which the Poisson's shrinkage effects can be neglected, the force, F_f, to overcome frictional pull-out in the debonded length, l_d, is given (see Appendix II) by

$$F_f = 2\pi a P_o\mu(L-l_u) \quad (6)$$

where P_o is the shrinkage pressure and μ is the coefficient of friction between fibre and matrix. The pull-out force, F_p, can readily be determined from Equations 5 and 6 using the relationship

$$F_p = F_{uy}+F_f \quad (7)$$

It has been shown [5] that the debonding force, F_p, is a maximum when the remaining length of the fibre–matrix interface which has not debonded, l_u, reaches a critical value, l_c. Hence, F_{pmax} (the maximum debonding force recorded in a force–displacement plot of a pull-out test) is obtained by substituting $l_u = l_c$ in Equations 5, 6 and 7

$$F_p = F_{uy}+2\pi a P_o\mu(L-l_c) \quad (8)$$

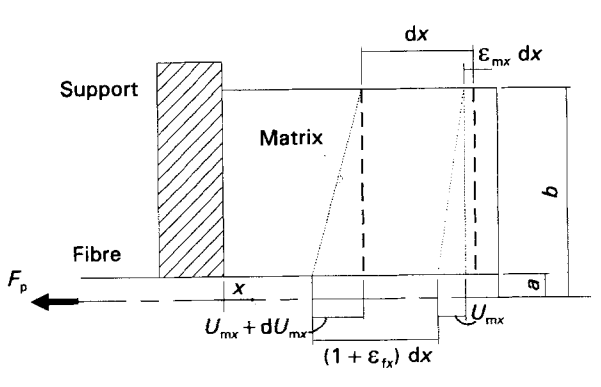

Figure 2 Elastic displacement of the fibre–matrix interface for restrained-top loading.

2.3. Effect of Poisson's shrinkage

When a ductile fibre or high aspect ratio fibre is used as a reinforcement component in a composite system, Poisson's effect will have a detectable influence on the debonding force. A high tensile stress on the fibre will result in a radial shrinkage in the fibre. This reduces the shrinkage pressure of the matrix on to the fibre and hence the frictional force, F_f, will be reduced. It can be shown (see Appendix II) that under these conditions, the pull-out force, F_p, is given by

$$F_p = \frac{\pi a^2 P_o}{K} + \left(F_{uy} - \frac{\pi a^2 P_o}{K}\right) e^{2\mu K(L - l_o)/a} \quad (9)$$

where $K = E_m \nu_f / E_f(1 + \nu_m)$, and ν_f and ν_m are the Poisson's ratios of the fibre and matrix, respectively.

3. Results and discussion

Differences in the effect of the moduli ratio, R (where $R = E_m/E_f$), and specimen dimensions on the stress distribution for both loading conditions will now be considered. From these, the influence of the above factors on the point of debonding crack initiation would be determined. Next, the dependence of the maximum pull-out force, F_{pmax}, and the critical fibre embedded length, l_c, on the loading condition would be elucidated. Finally, the influence of Poisson's effect and the interfacial shear strength on the variation of debonding force, F_{pmax}, with the fibre embedded length for the two loading conditions would be outlined. The pertinent equations for the fixed-bottom loading condition are available elsewhere [5].

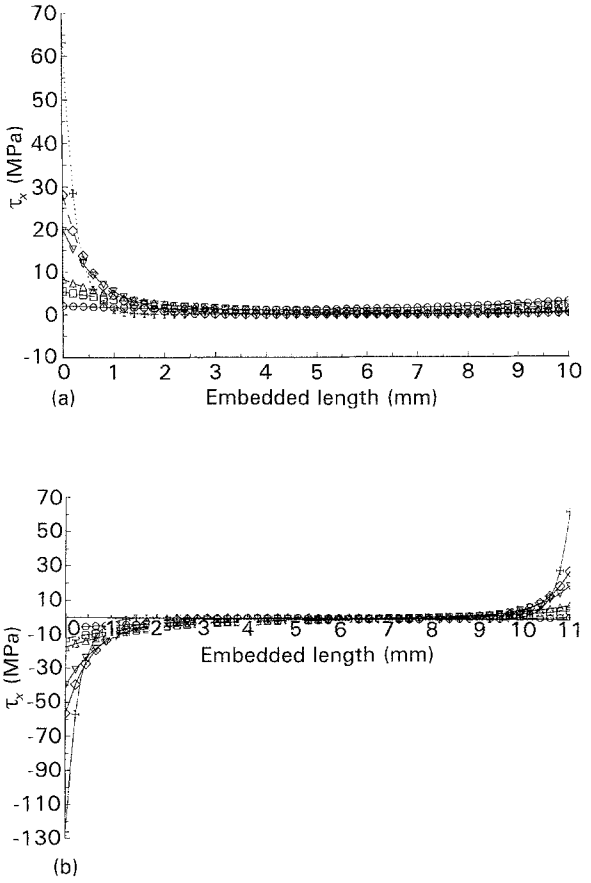

Figure 3 Variation of interfacial shear stress, τ_x, for (a) fixed bottom loading condition (FBC), and (b) restrained top loading condition (RTC). $R = E_m/E_f$: (○) 0.001, (□) 0.005, (△) 0.01, (▽) 0.05, (◇) 0.1, (+) 0.5.

3.1. Effect of modulus ratio, $R = E_m/E_f$, on the stress distribution

The effect of the modulus ratio, R, on the interfacial shear stress distribution and on the tensile stress distributions in the matrix and fibre for both loading conditions will now be considered. Plots of the stress distributions can be used to pin-point locations where failure initiation is likely to occur. To generate the plots in this section, the modulus of the matrix was varied while the fibre modulus, E_f, and the matrix and fibre diameters were fixed at 100 GPa, 2.5 and 0.1 mm, respectively. A pull-out force of 10 N was also assumed.

3.1.1. Effect on interfacial debonding

The plots of interfacial shear stress along the embedded length for the two loading conditions are as shown in Fig. 3. Debonding will initiate at the location where the interfacial shear stress is a maximum. It can be seen from Fig. 3 that the fibre emergent and embedded ends are points of high stress concentration. A clearer representation of the stress levels at the emergent and embedded ends is given in Fig. 4. The interfacial shear stress at the emergent end increases with increasing moduli ratio, R.

It can be seen from Fig. 4 that, for most values of R, the maximum interfacial shear stress, τ_x, exists at the emergent end ($x = 0$) for both loading conditions.

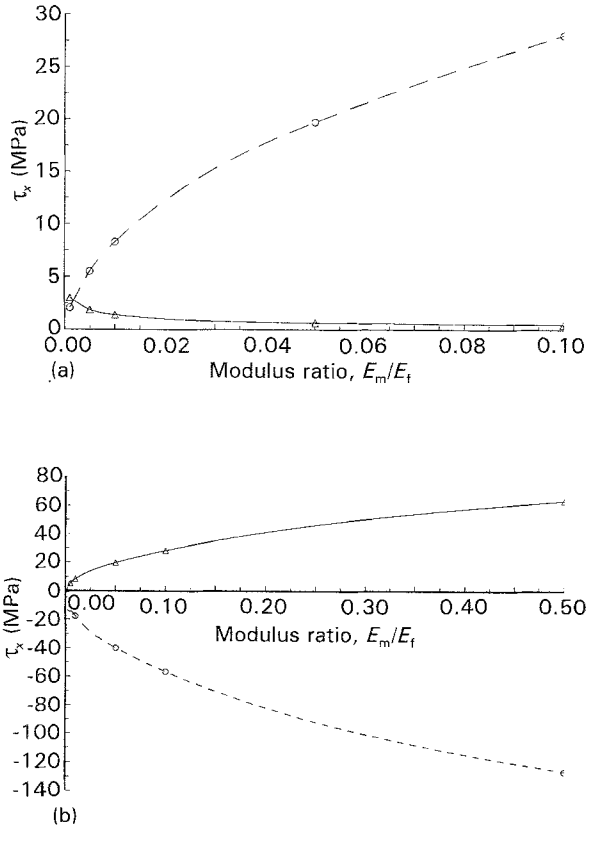

Figure 4 Interfacial shear stress, τ_x, at (---) emergent and (——) embedded end for (a) FBC, and (b) RTC.

However, for the FBC, τ_x is higher at the embedded end ($x = L$) for composite system with very low moduli ratio (see Fig. 4a). This implies that interfacial failure in most (thermoplastic, thermoset and carbon matrix-based) composite systems under both loading conditions is expected to initiate at the fibre emergent end. However, debonding in composite systems with low R($R < 0.002$), such as elastomer-based model systems, for the FBC will initiate at the fibre embedded end.

An interesting feature in Fig. 3 is that two points of stress concentration exist (at $x = 0, L$) for the RTC. In contrast, only one point of stress concentration exists for the FBC. In the RTC, the shear stresses at both ends act in opposite directions. The stress concentration at the emergent end ($x = 0$) is double that at the embedded end (see Fig. 3b). Although the magnitude of the stress concentration at the two ends is different, it is apparent that two debonding cracks can initiate within a specimen for the RTC. This is because defects commonly exist in practical specimens so that "simultaneous" debonding can occur at both ends of the fibre. Such simultaneous debonding at both ends has previously [13] been reported.

It is also important to note that, for any given system, the interfacial stress level is higher for the RTC than for the FBC (see Fig. 3). For a given applied load and R, the highest stress level in the former condition is about twice that for the latter condition. This can be attributed to the presence of compressive stresses within the matrix for the RTC which will be highlighted in a later section. A higher stress concentration for the RTC has also been predicted [11] for a model developed from a fracture-based approach.

3.1.2. Effect on matrix yielding

The stress distribution in the matrix, σ_{mx}, is as shown in Fig. 5. For the FBC (see Fig. 5a), σ_{mx} is tensile in nature. In contrast, the restrained-top loading mode has the effect of inducing compressive stresses within the matrix (see Fig. 5b). The size of the compressive zone in the matrix decreases as R is decreased. The cross-over point at which the stress changes from being tensile to compressive is further from the emergent end for smaller R. It can be seen from Fig. 5b that for most thermoplastic/thermoset glass/Kevlar/carbon fibre composites (which typically have $0.001 < R < 0.01$), the compressive matrix zone can occupy between 50% and 85% of the fibre embedded length.

It can be seen from Fig. 5 that σ_{mx} over the embedded length decreases with decreasing matrix modulus (i.e. decreasing R). It is apparent from Fig. 5 that stress transfer from the matrix to the fibre in the model composite is ineffective (i.e. high σ_{mx}) for $R > 0.05$ and is good for $R < 0.01$. This implies that stress transfer in composite systems with high R, such as carbon/carbon fibre composites, would be ineffective.

The difference in matrix stress state for the two loading conditions does not result in any difference in the magnitude of maximum σ_{mx} (see Fig. 5). However, the compressive stress state in the matrix for the RTC

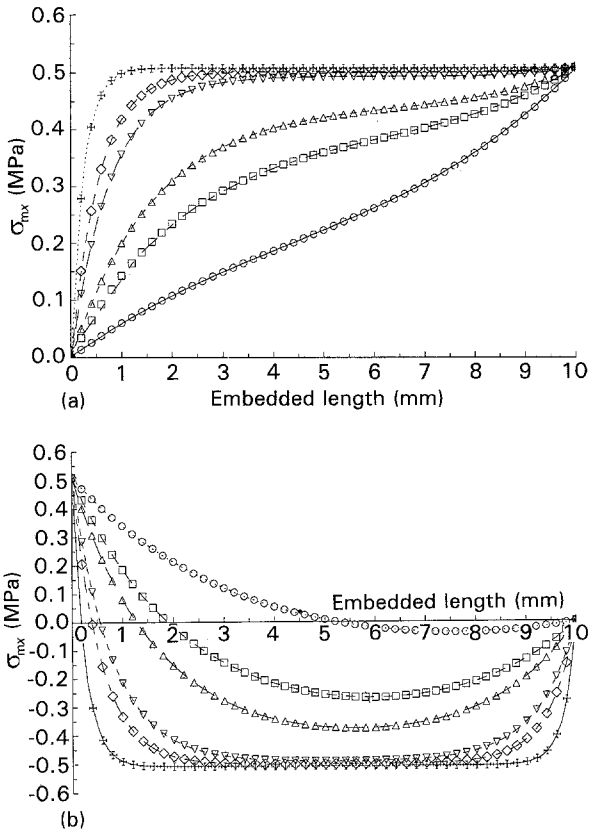

Figure 5 Variation of longitudinal stress of matrix, σ_{mx}, for (a) FBC, and (b) RTC. For key, see Fig. 3.

is responsible for the larger interfacial shear stress, τ_x (see Fig. 3), for this condition. For the RTC, the maximum value of the compressive stress has the same magnitude as the maximum tensile stress.

The implications of the variation of σ_{mx} along the embedded length on matrix yielding will now be considered. Failure initiation by matrix yielding is important in composite systems where $\tau_i > \sigma_{mx}$. Such a situation may sometimes exist where fibre surface treatments favour formation of a strong interface or interphase. For typical composite systems with $0.001 < R < 0.01$, σ_{mx} is maximum at the embedded end ($x = 0$) for the fixed-bottom specimen and at the emergent end ($x = L$) for the restrained-top specimen. Hence, the point of failure initiation is dependent on the loading method utilized.

For less common composite systems with $R > 0.05$, under the FBC, failure may initiate at any point in the high stress region which occupy more than 60% of the fibre embedded region (see Fig. 5a). In contrast, under the RTC, failure initiation by matrix yielding can only occur at the fibre emergent end (see Fig. 5b). Failure would not initiate from the compressive stress region because the polymer matrix is stronger in compression than in tension and $\sigma_{mx(max)}$ [tension] = $\sigma_{mx(max)}$ [compression].

3.1.3. Effect on fibre fracture

In practice, fibre fracture either at or just below the emergent surface would render the pull-out test void. Such fibre failure has been commonly observed [14]

experimentally. The likelihood for such fibre fracture will now be considered. Plots of the variation of σ_{fx} along the embedded fibre are as shown in Fig. 6. Two points of stress concentration exist in the RTC but only one such point exists in the FBC. It can be seen that σ_{fx} is maximum at the fibre emergent end ($x = 0$) for both forms of loading. This magnitude of $\sigma_{fx(max)}$ for the fixed-bottom (Fig. 6a) is five times higher than that of the restrained-top system (Fig. 6b). This indicates that the incidence of the fibre fracture at the emergent end of the pull-out specimen would be higher in the fixed-bottom loading condition. Therefore, in systems where the fibres are prone to fracture, the restrained-top loading condition is more likely to lead to a successful pull-out test.

3.2. Effect of specimen geometry

To elucidate the effect of specimen geometry on the ease and point of debonding initiation, the variation of interfacial shear stress levels at the embedded and emergent ends with geometry was determined for the composite systems in Table I. The glass fibre–polypropylene and glass fibre–rubber systems in Table I represent composite systems with medium ($R = 0.016$) and low ($R < 0.001$) moduli ratio, respectively.

In the first instance, the embedded length and the diameter of the matrix block were kept constant at 10 and 20 mm, respectively, while the fibre diameter was varied. The results are as shown in Fig. 7. It can be seen from Fig. 7b for the RTC that τ_x is higher at the emergent end for all fibre diameters. Hence, the point of debonding initiation is independent of fibre diameter for this loading condition. In contrast, for FBC (Fig. 7a), τ_x at the embedded end is higher when the fibre diameter is greater than 0.25 mm for $R = 0.016$. Thus, an emergent–embedded failure transition exists as the fibre diameter is increased. Moreover, τ_x at the embedded end is always higher when $R < 0.001$.

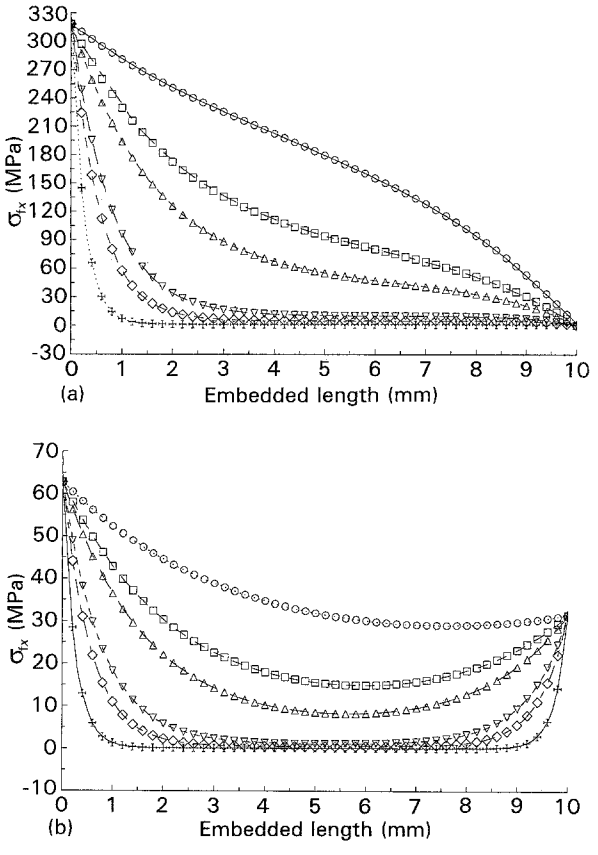

Figure 6 Variation of longitudinal stress of fibre, σ_{fx}, for (a) FBC, and (b) RTC. For key, see Fig. 3.

TABLE I Parameters of the composite system considered in the analysis

System	E_m(GPa)	E_f(GPa)	ν_m	ν_f
Glass fibre–PP	1.4	60.0	0.35	0.22
Glass fibre–rubber	0.002	60.0	0.5	0.22

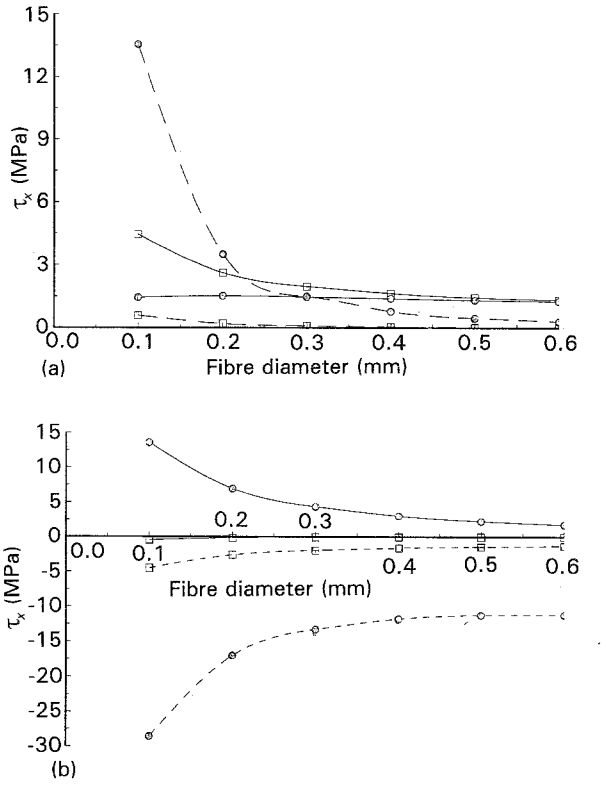

Figure 7 Effect of fibre diameter on the interfacial shear stress, τ_x, at the (---) emergent and (——) embedded end for (a) FBC, and (b) RTC. (●) pp/glass, (□) rubber/glass.

Next, the embedded length and the diameter of the fibre were kept constant at 10 and 0.1 mm, whilst the diameter of the matrix block was varied. The dependence of τ_x on the matrix diameter is as shown in Fig. 8. For the RTC, the general characteristics in Fig. 8b are similar to that in Fig. 7b. However, Fig. 8a for the FBC has some interesting features. For $R < 0.001$, τ_x at the embedded end is always higher. However, for $R = 0.016$, an embedded–emergent failure transition occurs as the matrix diameter is increased above 0.75 mm (see Fig. 8a). The above results clearly indicate that the point or location of interfacial debonding is affected by the fibre and matrix diameter and R for the FBC.

3.3. Pull-out force for interfacial debonding

To determine the effect of the loading system on the debonding force, F_p, and the maximum debonding

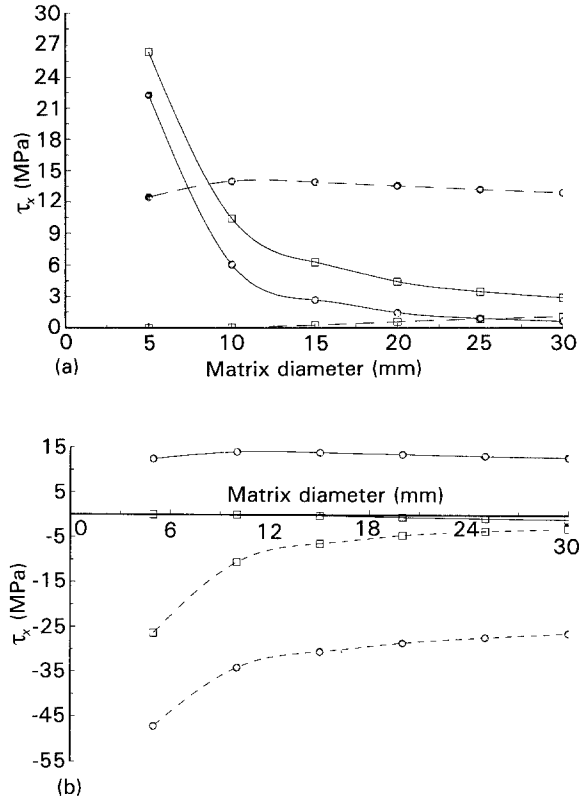

Figure 8 Effect of matrix diameter on the interfacial shear stress, τ_x, at the (---) emergent and (——) embedded end for (a) FBC, and (b) RTC. (●) pp/glass, (□) rubber/glass.

force in a pull-out test, F_{pmax}, the variation of F_p, F_{uy} and F_f during debonding crack propagation along the fibre embedded length will now be considered for the glass fibre/polypropylene system. In the analysis, the matrix and fibre diameters, the embedded length and the pull-out force were taken to be 2.5, 0.1 and 10 mm and 10 N, respectively. Equations 5–7 were utilized.

The change in F_p, V_{uy} and F_f with advancing crack front during crack propagation is as shown in Fig. 9. The debonding crack is initiated when τ_x is equal to τ_i. As the crack advances, the pull-out force F_{uy} decreases resulting in a corresponding drop in τ_x such that $\tau_x < \tau_i$. For the crack front to advance continuously, the shear stress at the crack tip must be kept at τ_i. This is achieved by maintaining F_{uy} at a constant critical value as shown in Fig. 9. However, when the remaining length of the fibre interface which is bonded, l_u, becomes less than a critical value, l_c, the force, F_{uy}, required to maintain the stress at the crack tip at τ_i falls rapidly (see Section 2.2). This is represented by the decrease in F_{uy} at large displacements of the debonding crack front in Fig. 9. If Poisson's effect is neglected, the contribution of frictional force F_f to F_p in the system increases linearly with the debonded fibre length during the debonding process (see Fig. 9).

The contribution of the frictional force component F_f to F_p is the same for both loading conditions. It can be seen from Fig. 9 that the debonding force F_{uy} for the RTC is half that obtained for the FBC. This can be attributed to the higher interfacial shear stress concentrations (see Section 3.1.1) for the former loading condition. The variation of F_p with the location of the advancing crack front is determined using Equation 7 and is represented in Fig. 9.

It can be seen from Fig. 9 that F_p for the FBC is higher than that for the RTC. In addition, $F_{p(max)}$ for the former condition is higher than that for the latter condition. However, the difference in $F_{p(max)}$ for the two conditions is small (see Fig. 9) despite the fact that the interfacial shear stress concentration in the RTC is double that for the FBC. The small difference observed is due to the fact that the frictional component F_f is dominant when $F_{p(max)}$ is reached.

3.4. Critical fibre embedded length

The critical fibre embedded length, l_c (Section 2.2), can be obtained by differentiating Equation 8 or 9 with respect to the bonded length and equating dF_p/dl_u to zero. Utilizing the parameters in Table I, l_c for the polypropylene/glass fibre system for the FBC and RTC were found to be 1.44 and 0.83 mm, respectively. Thus, in general, l_c for the RTC seem to be about half that for the FBC. The variation of l_c with R is as shown in Fig. 10. Therefore, l_c is dependent on the loading condition and on R.

3.5. Effect of Poisson's shrinkage

Fig. 11 shows the theoretical curves of F_p versus L for both types of loading with and without Poisson's effect for the PP/glass fibre system. It can be seen from

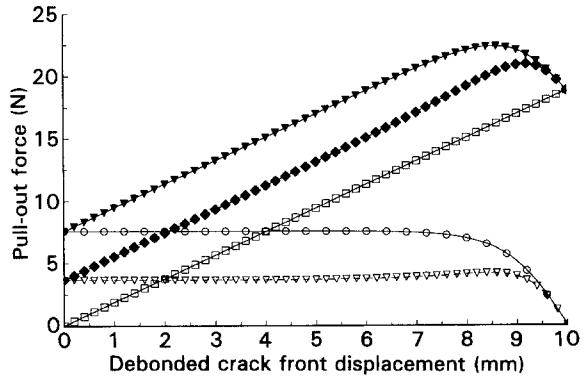

Figure 9 Variation of total pull-out force, F_p, frictional force, F_f and debonding force, F_{uy}, during the debonding process. (○) F_{uy}, FBC; (□) F_f, FBC and RTC; (▼) F_d, FBC; (▽) F_{uy}, RTC; (◆)F_d, RTC.

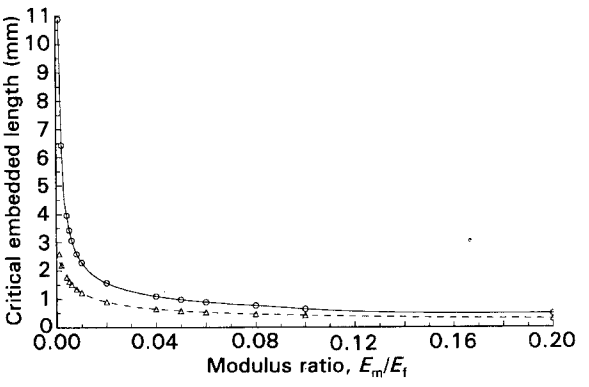

Figure 10 Variation of critical embedded length, l_c, with modulus ratio, $R = E_m/E_f$. (○) FBC, (△) RTC.

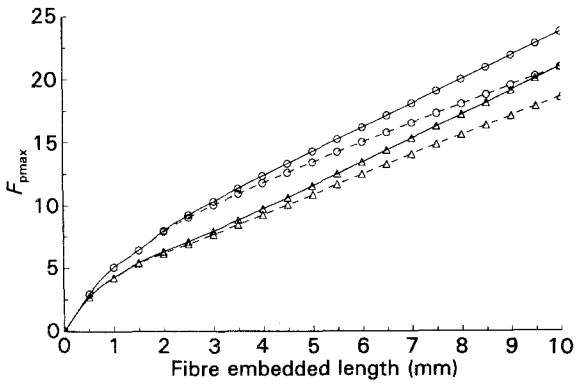

Figure 11 Effect of Poisson's shrinkage on the plot of F_{pmax} against the embedded length, L: (---) with and (——) without Poisson's shrinkage; (○) FBC, (△) RTC.

Fig. 11 that the effect of Poisson's shrinkage in the fibre is to change the slope of the curve by lowering $F_{p(max)}$ at $l > l_c$. For a given embedded fibre length, the magnitude of this effect is the same for both types of loading.

4. Conclusion

It can be seen that the stress distributions for τ_x, σ_{mx} and σ_{fx} along the fibre embedded length is dependent on the modulus ratio, R, the size of the fibre and matrix block, and the loading condition utilized in the pull-out test. This has important consequences on the ease and location of debonding crack initiation in the specimen. Fibre breakage occurs more readily in the fixed-bottom loading condition. For failure by matrix yielding, more possible points of failure initiation exist for the FBC. Interfacial failure initiates at a lower applied load in the restrained-top loading condition. The maximum pull-out force, $F_{p(max)}$ is higher for the FBC. However, the difference in $F_{p(max)}$ for the two loading conditions is not very large.

Appendix I

Consider a restrained-top pull-out system as shown in Fig. 1 subjected to a load. The radius of the cylinder and the fibre is depicted in Fig. 2. Neglecting the stress across the fibre end, it can be shown from the displacement considerations that

$$(1 + \varepsilon_{fx})dx + U_{mx} - (U_{mx} + dU_{mx}) + \varepsilon_{mx}dx = dx$$

so that

$$\frac{dU_{mx}}{dx} = \varepsilon_{fx} + \varepsilon_{mx} \quad \text{(A1)}$$

The fibre–matrix interface is subjected to a force system as shown in the free body diagram (Fig. 2).

For force equilibrium of the matrix

$$\tau_x = \frac{(b^2 - a^2)}{2a}\frac{d\sigma_{mx}}{dx} \quad \text{(A2)}$$

and for the fibre

$$\tau_x = \frac{a}{2}\frac{d\sigma_{fx}}{dx} \quad \text{(A3)}$$

At any cross-section of the system it can be shown that

$$F_p = \pi a^2\sigma_{fx} - \pi(b^2 - a^a)\sigma_{mx} \quad \text{(A4)}$$

The displacement, U_{mx}, can be written as

$$U_{mx} = \int_a^b \frac{\tau_y}{G_m}dy \quad \text{(A5)}$$

where τ_y is the shear stress at a distance y from the centre of the fibre–matrix system shown in Fig. 2.

For a free surface, the shear stress at the circumference is zero. Assuming that the shear force decreases linearly in the y-direction from S_i at the interface to 0 at the circumferential surface of the matrix. The shear force, S_i, at the interface ($r = a$) is

$$S_i = 2\pi a\tau_x dx$$

and at a distance y

$$\tau_y = \tau_x\frac{a}{y}\left(\frac{b - y}{b - a}\right) \quad \text{(A6)}$$

Substituting Equation A6 into A5 gives

$$U_{mx} = \int_a^b \frac{\tau_x}{G_m}\frac{a}{y}\left(\frac{b - y}{b - a}\right)dy$$

$$= \frac{\tau_x a}{G_m}\left[\frac{b}{b - a}\ln\left(\frac{b}{a}\right) - 1\right] \quad \text{(A7)}$$

Differentiating Equations A2 and A7 with respect to x gives

$$\frac{d\tau_{mx}}{dx} = \left(\frac{b^2 - a^2}{2a}\right)\frac{d^2\sigma_{mx}}{dx} \quad \text{(A8)}$$

and

$$\frac{dU_{mx}}{dx} = \frac{a}{G_m}\left[\frac{b}{(b - a)}\ln\left(\frac{b}{a}\right) - 1\right]\frac{d\tau_x}{dx} \quad \text{(A9)}$$

Substituting Equation A8 into A9

$$\frac{dU_{mx}}{dx} = \frac{(b^2 - a^2)}{2G_m}\left[\frac{b}{b - a}\ln\left(\frac{b}{a}\right) - 1\right]\frac{d^2\sigma_{mx}}{dx^2} \quad \text{(A10)}$$

From the theory of elasticity, Equation A1 can be written as

$$\frac{dU_{mx}}{dx} = \frac{\sigma_{fx}}{E_f} + \frac{\sigma_{mx}}{E_m} \quad \text{(A11)}$$

Substituting Equation A11 into Equation A10 gives

$$\frac{d^2\sigma_{mx}}{dx^2} = 2G_m\Big/\left\{(b^2 - a^2)\left[\left(\frac{b}{b - a}\right)\ln\left(\frac{b}{a}\right) - 1\right]\right\} \times\left[\frac{\sigma_{fx}}{E_f} + \frac{\sigma_{mx}}{E_m}\right] \quad \text{(A12)}$$

From Equation A4

$$\sigma_{fx} = \frac{F_p + \pi(b^2 - a^2)\sigma_{mx}}{\pi a^2}$$

$$= \frac{1}{a^2}\left[\frac{F_p}{\pi} + (b^2 - a^2)\sigma_{mx}\right] \quad \text{(A13)}$$

Substituting this into Equation A12 gives

$$\frac{d^2\sigma_{mx}}{dx^2} = 2G_m\Big/\left\{(b^2 - a^2)\left[\left(\frac{b}{b-a}\right)\ln\left(\frac{b}{a}\right) - 1\right]\right\}\left\{\frac{1}{E_f a^2}\left[-\frac{F_p}{\pi} + (b^2 - a^2)\sigma_{mx}\right] + \frac{\sigma_{mx}}{E_m}\right\}$$

$$= 2G_m\Big/\left\{(b^2 - a^2)\left[\left(\frac{b}{b-a}\right)\ln\left(\frac{b}{a}\right) - 1\right]\right\}\left[\frac{E_m(b^2 - a^2) + E_f a^2}{E_f E_m a^2}\right]\sigma_{mx}$$

$$+ 2G_m F_p\Big/\left\{(b^2 - a^2)\left[\left(\frac{b}{b-a}\right)\ln\left(\frac{b}{a}\right) - 1\right]\pi a^2 E_f\right\} \quad \text{(A14)}$$

Equation A14 is of the form

$$\frac{d^2\sigma_{mx}}{dx^2} = A\sigma_{mx} + B$$

where

$$A = 2G_m\Big/\left\{(b^2 - a^2)\left[\left(\frac{b}{b-a}\right)\ln\left(\frac{b}{a}\right) - 1\right]\right\}\left[\frac{E_m(b^2 - a^2) + E_f a^2}{E_f E_m a^2}\right]$$

$$B = 2G_m F_p\Big/\left\{(b^2 - a^2)\left[\left(\frac{b}{b-a}\right)\ln\left(\frac{b}{a}\right) - 1\right]\pi a^2 E_f\right\}$$

The solution to Equation A14 is

$$\sigma_{mx} = \frac{F_p}{\pi(b^2 - a^2)}\left[\frac{(1 + \psi)\sinh\alpha(L - x) + \psi\sinh(\alpha x)}{\sinh(\alpha L)} - \psi\right] \quad \text{(A15)}$$

The stress distribution of the fibre can be obtained by substituting Equation A15 into Equation A13

$$\sigma_{fx} = \frac{F_p}{\pi a^2}\left[1 + \frac{(1 + \psi)\sinh\alpha(L - x) + \sinh(\alpha x)}{\sinh(\alpha L)} - \psi\right] \quad \text{(A16)}$$

Differentiating Equation A15 with respect to x and substituting this into Equation A3 gives

$$\frac{d\sigma_{fx}}{dx} = \frac{F_p}{\pi a^2}\left[\frac{-\alpha(1 + \psi)\cosh\alpha(L - x) - \alpha\psi\cosh(\alpha x)}{\sinh(\alpha L)}\right] \quad \text{(A17)}$$

$$\tau_x = \frac{F_p}{2\pi a}\left[\frac{-\alpha(1 + \psi)\cosh\alpha(L - x) + \alpha\psi\cosh(\alpha x)}{\sin(\alpha L)}\right] \quad \text{(A18)}$$

Appendix II

Pull-out against friction

Consider a specimen in the restrained-top loading configuration shown in Fig. A1. Assume that the fibre is rigid and the matrix is elastic. For equilibrium of forces on the fibre element of length dl (see Fig. A2),

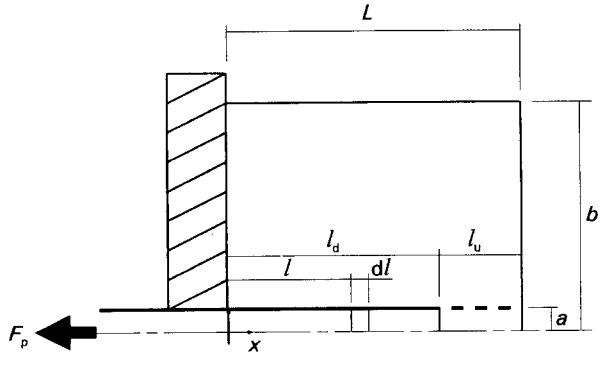

Figure A1 Partial debonding of fibre embedded specimen.

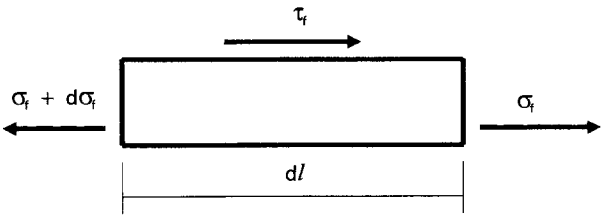

Figure A2 Elemental of length, dl, of the debonded region.

within the debonded region of the fibre–matrix interface

$$\frac{d\sigma_f}{dl} = \frac{2\tau_f}{a} \quad \text{(A19)}$$

where τ_f is the frictional stress on the interface, σ_f is the tensile stress of the fibre. The value of τ_f is dependent on the shrinkage pressure of the matrix P_o and the interfacial coefficient of friction μ, where $\tau_f = \mu P_o$. Substituting this into Equation A19

$$\frac{d\sigma_f}{dl} = \frac{2P_o\mu}{a} \quad \text{(A20)}$$

The frictional force over the debonded region can be obtained by intergrating Equation A20 over the debonded region. That is

$$F_f = \pi a 2\mu P_o(L - l_d) \quad \text{(A21)}$$

Effect of Poisson's shrinkage on the fibre

In the case of a ductile fibre or fibre with high aspect ratio, Poisson's shrinkage is significant if the tensile stress of the fibre is high. Poisson's shrinkage reduces the shrinkage pressure on the fibre thus decreasing the interfacial friction. Because the tensile stress of the fibre varies along the embedded length, a similar variation of Poisson's effect occurs. The radial shrinkage strain, ε_r, of the fibre is

$$\varepsilon_r = \frac{\sigma_f \nu_f}{E_f} \quad \text{(A22)}$$

The thick cylinder theory can be applied to determine the drop in shrinkage pressure due to Poisson's shrinkage. Substituting the radial shrinkage strain of Equation A22 into thick cylinder theory gives a pressure drop of

$$P_d = \frac{E_m \nu_f \sigma_f}{E_f(1 + \nu_m)} \quad \text{(A23)}$$

Therefore, the frictional stress becomes

$$\tau_f = \left[P_o - \frac{E_m \nu_f \sigma_f}{E_f(1 + \nu_m)}\right]\mu = (P_o - K\sigma_f)\mu \quad \text{(A24)}$$

where $K = E_m \nu_f / E_f(1 + \nu_m)$. Substituting Equation A24 into A19 and rearranging

$$\frac{d\sigma_f}{dl} + \frac{2\mu K}{a}\sigma_f = \frac{2\mu P_o}{a} \quad \text{(A25)}$$

The above is a first-order differential equation and its solution is

$$e^{2\mu K l/a}\sigma_f = \frac{P_o}{K} e^{2\mu K l/a} + C \quad \text{(A26)}$$

The constant C can be evaluated from the boundary condition $\sigma_f = 0$ at $l = -(L - l_u)$. It can be shown for the case where the fibre has debonded a length, l_d, pull-out force due to friction, F_f, is given by

$$F_f = \frac{\pi a^2 P_o}{K}(1 - e^{2\mu K(L - l_u)/a}) \quad \text{(A27)}$$

Effect of friction in the debonding process

During the debonding process, the embedded length is comprised of the debonded, l_d, and the bonded regions (see Fig. A2). Poisson's shrinkage will only affect the debonded region. The tensile force, F_x, can be obtained by multiplying Equation A26 by the cross-sectional area of the fibre so that

$$F_x e^{2\mu K l/a} = \frac{2\pi a^2 P_o}{K} e^{2\mu K l/a} + D \quad \text{(A28)}$$

Using the boundary condition, $F_x = F_{uy}$ at $l = (L - l_u)$ the constant D in Equation A28 can be evaluated and the pull-out force is given by

$$F_p = \frac{\pi a^2 P_o}{K} + \left[F_{uy} - \frac{\pi a^2 P_o}{K}\right] e^{2\mu K(L - l_u)/a} \quad \text{(A29)}$$

References

1. A. KELLY and W. R. TYSON, *J. Mech. Phys. Solids* **13** (1965) 329.
2. P. LAWRENCE, *J. Mater. Sci.* **7** (1972) 1.
3. A. TAKAKU and R. G. C. ARRIDGE, *J. Phys. D Appl. Phys.* **6** (1973) 2038.
4. C. H. HSUEH, *Mater. Sci. Eng.* **A130** (1990) L11.
5. C. Y. YUE and W. L. CHEUNG, *J. Mater. Sci.* **27** (1992) 3173.
6. C. GURNEY and J. HUNT, *Proc. R. Soc.* **A299** (1967) 508.
7. J. K. WELLS and P. W. R. BEAUMONT, *J. Mater. Sci.* **23** (1988) 1274.
8. H. STANG and S. P. SHAH, *ibid.* **21** (1986) 953.
9. L. M. ZHOU, J. K. KIM and Y. W. MAI, *ibid.* **27** (1992) 3155.
10. C. Y. YUE and W. L. CHEUNG, *J. Mater. Sci. Lett.* **10** (1991) 1335.
11. L. M. ZHUO, J. K. KIM and Y. W. MAI, *Compos. Sci. Technol.* **45** (1992) 153.
12. C. Y. YUE and W. L. CHEUNG, *J. Mater. Sci.* **27** (1992) 3181.
13. J. BOWLING and G. W. GROVES, *ibid.* **14** (1979) 431.
14. C. Y. YUE, unpublished data (1988).

Received 24 May
and accepted 29 October 1993